



HAL
open science

Quantification of silanol sites for the most common mesoporous ordered silicas and organosilicas: total versus accessible silanols

Matthias Ide, Mohamad El-Roz, Els de Canck, Aurélie Vicente, Tom Planckaert, Thomas Bogaerts, Isabel van Driessche, Frederic Lynen, Veronique van Speybroeck, Frédéric Thybault-Starzyk, et al.

► To cite this version:

Matthias Ide, Mohamad El-Roz, Els de Canck, Aurélie Vicente, Tom Planckaert, et al.. Quantification of silanol sites for the most common mesoporous ordered silicas and organosilicas: total versus accessible silanols. *Physical Chemistry Chemical Physics*, 2013, 15 (2), pp.642-650. 10.1039/c2cp42811c . hal-01963802

HAL Id: hal-01963802

<https://hal.science/hal-01963802v1>

Submitted on 5 Oct 2021

HAL is a multi-disciplinary open access archive for the deposit and dissemination of scientific research documents, whether they are published or not. The documents may come from teaching and research institutions in France or abroad, or from public or private research centers.

L'archive ouverte pluridisciplinaire **HAL**, est destinée au dépôt et à la diffusion de documents scientifiques de niveau recherche, publiés ou non, émanant des établissements d'enseignement et de recherche français ou étrangers, des laboratoires publics ou privés.

Quantification of Silanol Sites for the Most Common Mesoporous Ordered Silicas and Organosilicas: Total Versus Accessible Silanols.

Journal:	<i>The Journal of Physical Chemistry</i>
Manuscript ID:	jp-2012-050884
Manuscript Type:	Article
Date Submitted by the Author:	25-May-2012
Complete List of Authors:	<p>Ide, Matthias; University of Ghent, Inorganic and Physical Chemistry El-Roz, Mohamad; ENSICAEN, Université de Caen, CNRS , Laboratoire Catalyse et Spectrochimie De Canck, Els; Ghent University, Inorganic and Physical Chemistry Vicente, Aurelie; ENSICAEN, Université de Caen, CNRS, Laboratoire Catalyse et Spectrochimie Planckaert, Tom; University of Ghent, Inorganic and Physical Chemistry Bogaerts, Thomas; University of Ghent, Inorganic and Physical Chemistry Lynen, Frederic; Ghent University, Organic chemistry Van Speybroeck, Veronique; Ghent University, Center for Molecular Modeling Thibault-Starzyk, Frederic; CNRS, ENSICAEN - Laboratoire Catalyse et Spectrochimie Van Der Voort, Pascal; Ghent University, Department of Inorganic and Physical Chemistry</p>

SCHOLARONE™
Manuscripts

1
2
3
4
5
6
7
8
9
10
11
12
13
14
15
16
17
18
19
20
21
22
23
24
25
26
27
28
29
30
31
32
33
34
35
36
37
38
39
40
41
42
43
44
45
46
47
48
49
50
51
52
53
54
55
56
57
58
59
60

Quantification of silanol sites for the most common mesoporous ordered silicas and organosilicas: total versus accessible silanols.

Matthias Ide,^a Mohamad El-Roz^b, Els De Canck^a, Aurélie Vicente^b, Tom Planckaert^a, Thomas Bogaerts^{a,e}, Isabel Van Driessche^c, Frédéric Lynen^d, Veronique Van Speybroeck^e, Frédéric Thybault-Starzyk^b and Pascal Van Der Voort^{a,}*

^aCOMOC, Center for Ordered Materials, Organometallics and Catalysis, Department of Inorganic and Physical Chemistry, Ghent University, Krijgslaan 281 (S-3), 9000 Ghent, Belgium. Fax: +32 9264 4983, Tel: +32 9264 4442

^bLaboratoire Catalyse et Spectrochimie (LCS), Université de Caen, 6, Bd du Marechal Juin, 14050 Caen Cedex, France.

^cDepartment of Inorganic and Physical Chemistry, Sol-gel Centre for Research on Inorganic Powder and Thin film Synthesis, University of Ghent, Krijgslaan 281 (S-3), 9000 Ghent, Belgium.

^dDepartment of Organic Chemistry, Laboratory of Separation Sciences, University of Ghent, Krijgslaan 281 (S-4), 9000 Ghent, Belgium.

^eCenter for Molecular Modeling, Ghent University, Technologiepark 903, B-9052 Zwijnaarde, Belgium.

E-mail: Pascal.Vandervoort@ugent.be

1
2
3
4
5
6
7
8
9
10
11
12
13
14
15
16
17
18
19
20
21
22
23
24
25
26
27
28
29
30
31
32
33
34
35
36
37
38
39
40
41
42
43
44
45
46
47
48
49
50
51
52

RECEIVED DATE (to be automatically inserted after your manuscript is accepted if required according to the journal that you are submitting your paper to)

IR and NMR spectroscopy were used to characterize the silanol content in the most common mesoporous ordered silicas: MCM-41, MCM-48 SBA-15 and SBA-16. The *total* silanol number and the amount of surface silanols, which can be reached by various common chromatographic silanes, are calculated for the most widespread mesoporous templated silicas (MTS). In addition, a comparison between MCM-41 prepared by spray dried synthesis (MCM-41(SD)) and by hydrothermal synthesis (MCM-41) has been performed in order to present the effect of the synthesis methods on the MCM-41 properties. The characterization of an ethene bridged Periodic Mesoporous Organosilica (PMO) is discussed in this paper. The results were compared with those of Nucleosil used as commercial silica material. The complete distribution of surface and bulk silanols, and of isolated, geminal and vicinal silanols for all these materials is presented. To complete the research and obtain a deeper understanding of the grafting reactions, theoretical calculations were performed to determine the geometry of the carbon substituents. There are distinct differences in the silanol contents and distribution of all these materials; we show that these differences are mostly due to the synthesis conditions, the pore architecture and the wall thickness. Remarkably, unlike silica gels or silica sols, up to 70% of the silanols on ordered mesoporous silicas and more than 90% of the silanols of a mesoporous organosilica is not accessible for small silanes.

53
54
55
56
57
58
59
60

KEYWORDS: Silanol number, ordered mesoporous materials, grafting, spray dried

Introduction

The silanol number is a topic of interest and discussion since the 1950s until today. A good knowledge of the number of silanols on the silica surface is important in areas such as catalysis and adsorption. Also in emerging disciplines, such as drug delivery, tissue engineering by silica and organosilica scaffolds, thin film technology, etc. , the exact knowledge of the silanol number is needed or at least desirable. More specifically, in the field of chromatography, the silanol groups are of major importance for two reasons. In the first place, they are the anchoring point for the stationary phase functional groups. In this way, they have a direct influence on the retention mechanism of a chromatographic packing material. Secondly, once the functional groups are grafted on the silica surface, it is important that the residual silanol groups are removed from the system by endcapping with e.g. a trimethylsilyl group. This, because residual silanol groups can, for example, lead to asymmetric or tailing signals in the chromatography of basic compounds. On the other hand, in a technique such as capillary electrochromatography (CEC) the remaining silanol groups help to create the electro osmotic flow, which drives the separation. [1]

The determination of the silanol number is complicated by the easy adsorption of water on silica. Therefore the exact quantification with MAS NMR, FTIR, selective chemisorption, deuterium exchange and mass spectroscopy is always complicated by the need for a very controlled atmosphere during sample treatment and measurement. Many models appeared in the 1970s and 80s on the determination of the silanol number of silica gels or fumed silicas.[2-4] For silica gels, many different datasets on the silanol number are available, with a large number originating from the former USSR. The silanol number is often referred to as the Zhuravlev number, in honor of his pioneering work in the field.[5-8] In 1995, Van Der Voort et al. published an overview of the silanol number of silica gels as a function of temperature with a specification of the number of isolated, geminal and vicinal silanols.[9] However for the mesoporous ordered (organo)silica

1 materials, prepared by anionic, cationic or neutral templates at a wide range of pHs and
2 temperatures, this table is no longer applicable, as we will show in this work.
3

4
5 Several standard methods have been used to characterize and quantify the density of silanol
6 groups of both amorphous and mesostructured silica materials. Thermogravimetric analyses[10],
7 diffuse reflectance fourier transform infrared spectroscopy (DRIFT) [11-12], ^{29}Si and ^1H NMR [13-
8 14], microcalometry [15] or a combination of these techniques were combined with the use of
9 probing molecules such as silanes [16-19], water [20-22] or pyridine [23] adsorption. The silanol
10 concentrations that have been reported on MCM-41 are hardly comparable, due the fact that each
11 paper reports a different silanol number for MCM-41 without considering synthesis and analysis
12 parameters. [24-29] For example the silanol number is strongly dependent on the temperature of
13 any post synthesis treatment. [9] However in six different reports where MCM-41 was post
14 treated at the same temperature, silanol values varying from 0.9 up to 3 groups per nm^2 were
15 found. [10, 23, 30-33] After a thorough search of literature no systematic determination of the
16 silanol number of periodic mesoporous organosilicas could be found. Also a systematic
17 comparison of the most common mesoporous ordered silicas is not available in literature.
18
19

20
21 Therefore in this contribution, we report the *accessible surface silanols* for various
22 chromatographic relevant functional groups together with the *total amount of silanol groups*,
23 whether they are on the surface or not. We believe this information will be useful for many
24 colleagues in various fields of research and for the chromatographic colleagues in particular. The
25 silanol numbers have been quantified using previously described IR techniques [34] combined
26 with solid state NMR and elemental analysis of grafting procedures.
27
28
29
30
31
32
33
34
35

36 37 38 39 40 41 42 43 44 45 46 47 48 49 50 51 52 53 2 Experimental

54 55 56 57 58 2.1 Materials

59
60

1 Nucleosil 300-5 (mean pore diameter: 30 nm; 5 μ m particle size) was purchased from Macherey-
2 Nagel. Hexadecyltrimethylammonium bromide (99%) (CTAB), tetraethyl orthosilicate (98%
3 reagent grade) (TEOS), ammonium hydroxide, potassium chloride (>99%) acetonitrile (HPLC
4 grade), 1-butanol (99.8%), pluronic PEO₂₀PPO₇₀PEO₂₀ (P123), pluronic PEO₁₀₆PPO₇₀PEO₁₀₆
5 (F127), Vinyltriethoxysilane (VTES) and Grubbs' 1st generation were acquired at Sigma-Aldrich.
6
7 Fuming hydrochloric acid 37 w/w% was purchased from Roth, anhydrous toluene (> 99,9%) for
8 the grafting was obtained from Acros. n-Octadecyldimethylchlorosilane(97%), n-
9 Octyldimethylchlorosilane and Bis(trimethylsilyl) amine were supplied by ABCR. All chemicals
10 were used without further purification.
11
12
13
14
15
16
17
18
19
20
21
22
23

24 2.2 Synthesis of the supports

25
26 SBA-15 [35], SBA-16 [36], MCM-41 [37], MCM-48 [38], spray dried MCM-41 [39] and ethene
27 bridged periodic mesoporous organosilica (PMO) [40] were all prepared according to methods
28 found in literature. All syntheses were carried out under hydrothermal conditions, except for the
29 spray dried MCM-41 type material, denoted as MCM-41 (SD). Two types of pore systems were
30 synthesized, a hexagonal and a cubical pore system. MCM-41, MCM-41(SD), SBA-15 and the
31 ethene bridged PMO have a hexagonal pore system. The MCM-48 and the SBA-16 both exhibit a
32 cubical pore system. All the synthesis procedures can be found in the supplementary information.
33
34 Nucleosil 300-5 is commonly used as a packing material in chromatographic HPLC applications.
35
36 MCM-41, MCM-41(SD), MCM-48, SBA-15 and SBA-16 were calcined at 550 °C for 6 hours with a
37 heating rate of 1.5°C/min to remove the surfactant. The surfactant of the ethene bridged PMO was
38 removed by a soxhlet extraction with acetone at 120 °C. [41] After the synthesis all the samples
39 were kept dry and under inert atmosphere.
40
41
42
43
44
45
46
47
48
49
50
51
52
53
54
55
56
57

58 2.3 Grafting procedures

1 Prior to grafting water was removed from the samples by a heating procedure at 120°C under
2 vacuum conditions for 24 hours.
3

4
5 Three different silanes with increasing tail length were used as probing molecules to determine
6 the amount of accessible silanol sites on the surface of the different silica materials. A
7 trimethylsilyl (C3), an octyldimethylsilyl (C8) and an octadecyldimethylsilyl (C18) group were
8 anchored to the surface. The reaction time was 24h for all the grafting reactions and the
9 composition of the final mixture was 0.5 g silica/1.4 mmol silane/30 ml solvent. The trimethylsilyl
10 and the octyldimethylsilyl group were grafted by means of hexamethyldisilazane and
11 octyldimethylchlorosilane, respectively, in dry acetonitrile and left to stir for 24 hours at room
12 temperature. The octadecyldimethylsilyl group was grafted by means of
13 octadecyldimethylchlorosilane in dry toluene under the same conditions as cited above.
14
15
16
17
18
19
20
21
22
23
24
25
26

27 After reaction the materials were filtered off, washed thoroughly with acetonitrile or toluene
28 and acetone, dried at 120°C under vacuum and analyzed with elemental analysis.
29
30
31
32
33

34 2.4 Characterization

35
36
37
38

39 Nitrogen adsorption experiments were measured at -196 °C using a Belsorp mini II gas analyzer.
40 X- ray powder diffraction (XRPD) patterns were collected on an ARL X'TRA X-ray diffractometer
41 with Cu K α radiation of 0.15418 nm wavelength and a solid-state detector. Elemental analyses (C,
42 H, N) were performed on a Thermo Scientific Flash 2000 CHNS-O Analyzer.
43
44
45
46
47

48 For the determination of the silanol number, a special transmission FTIR setup was used.
49
50
51
52
53
54
55
56
57
58
59
60

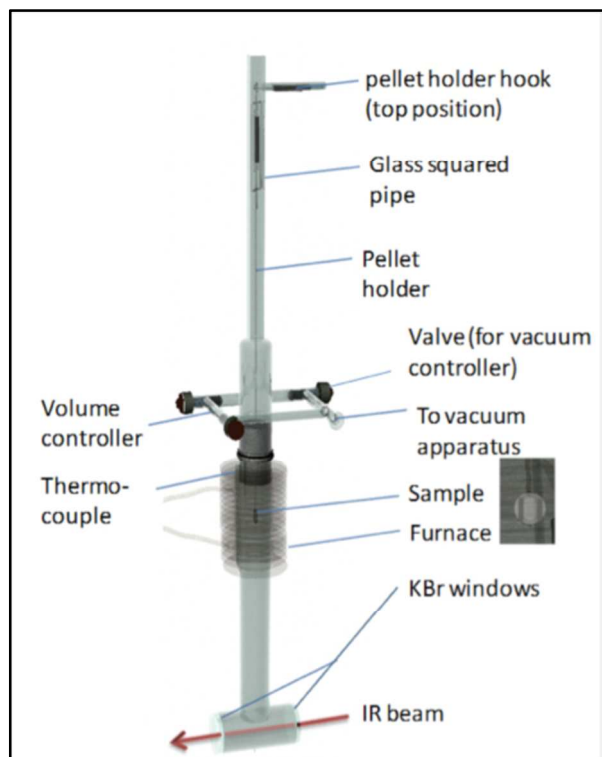


Figure 1: The In-Situ IR-cell used to determine the silanol number of the materials.

The silica powders were pressed ($\sim 10^7$ Pa) into self-supported discs (2 cm^2 area, $7\text{-}8 \text{ mg/cm}^2$). They were placed in a cell equipped with KBr windows. A movable quartz sample holder allowed placing the pellet in the infrared beam, for recording spectra, and moving it into a furnace at the top of the cell for thermal treatment (see figure 1).

A Nicolet 6700 IR spectrometer equipped with a DTGS detector and an extended-KBr beam splitter was used for the acquisition of spectra recorded in the $400\text{-}5500 \text{ cm}^{-1}$ range. Spectra were recorded at 4 cm^{-1} and 250 scans were co-added for each spectrum.

Solid-state MAS NMR spectra were recorded on a Bruker Avance-400 (9.4T) spectrometer using 4 mm-OD zirconia rotors and a spinning frequency of 12 kHz. Single pulse excitation (30° flip angle) and 20 s recycling delay was used for ^{29}Si MAS NMR experiments. $\{^1\text{H}\}\text{-}^{29}\text{Si}$ cross-polarization (CP) MAS experiments were performed using a contact time of 6 ms and a recycle time of 3 s. Tetramethylsilane (TMS) was used as chemical shift reference ^{29}Si nuclei.

3. Results and discussion

In order to simplify the discussion of the effect of the synthesis method on the material properties, the main differences between synthesis conditions and template removal are summarized in Table 1.

Table 1: Overview of the materials: synthesis conditions and template removal.

	Synthesis conditions		Template removal
SBA-15	Hydrothermal	Acid	Calcination
SBA-16	Hydrothermal	Acid	Calcination
MCM-41	Hydrothermal	Base	Calcination
MCM-48	Hydrothermal	Base	Calcination
MCM-41(SD)	Spray dried	Acid	Calcination
EthenePMO	Hydrothermal	Acid	Extraction

As mentioned above in the experimental part, the template removal has been performed by conventional calcination at 550°C, except the PMO which was activated by soxhlet extraction at 120°C using acetone as solvent. The comparison of the MCM-41 and MCM-41(SD) allows understanding the effect of hydrothermal and spray dried synthesis on the material behavior. For comparison, Nucleosil was purchased from Macherey-Nagel in order to be used as reference.

3.1 The pore properties of the materials

Three types of pore structures were synthesized, a hexagonal P6/mm structure (MCM-41-HT, MCM-41-SD, SBA-15 and ethene bridged PMO) and two cubical structures (MCM-48 (Ia3d) and SBA-16 (Im3m)). Additionally there are substantial differences between MCM type materials and SBA type materials in general. MCM type materials exhibit pore sizes between 2 and 4 nm with a wall thickness of about 1 nm. No significant difference in the pore properties can be discerned between the hydrothermally synthesized and the spray dried MCM-41 material. This is small compared to the SBA and PMO materials where pore sizes vary between 6 and 10 nm with a wall thickness between 3 and 7 nm. This difference in pore size properties can be assigned to the use of a different surfactant as pore generating agent. An additional property of the materials

synthesized with Pluronic surfactants is that next to mesopores also micropores are generated in the walls.

The various pore properties are shown in table 2, the surface area (SA_{BET}), pore volume (V_p) and pore diameter (d_p) were determined with N_2 -sorption. The unit cell (a_0) was determined from the XRD spectra of the materials and the wall thickness (h) was calculated with the following formulas:

$$\text{MCM-41, SBA-15 and ethene bridged PMO[42]: } h = a_0 - 0.95 d_p ;$$

$$\text{MCM-48[43]: } h = \frac{a_0}{3.0919} - \frac{d_p}{2} ;$$

$$\text{SBA-16[44]: } h = \frac{\sqrt{3}}{2} a_0 - d_p ;$$

Note that for Nucleosil no pore diameter could be calculated due to its broad pore size distribution. This material is also unordered, and does not produce any XRD reflections.

Table 2: The pore properties of the various materials, with SA_{BET} the surface area, V_p the pore volume, d_p the pore diameter, a_0 the unit cell and h the wall thickness.

Material	SA_{BET}	V_p	d_p	a_0	h
	m^2/g	cm^3/g	nm	nm	nm
SBA-15	656	0.7	6.9	10.7	4.2
SBA-16	738	0.6	6.2	14.6	6.4
MCM-41	1144	0.6	2.9	3.8	1.1
MCM-48	1293	0.8	2.8	7.3	1.0
MCM-41(SD)	719	0.4	2.9	3.6	1.2
EthenePMO	923	1.0	6.2	9.0	3.1
Nucleosil	88	0.4	-	-	-

3.2 The total concentration of silanol-groups from in-situ IR

According to the literature [34], adsorbed water species are characterised by a $\delta\text{H}_2\text{O}$ band near 1630 cm^{-1} (Figure 2 - a). The spectrum of the dried sample (Figure 2 - b) presents a narrow band at 3740 cm^{-1} characterizing isolated silanol groups. The band of inner hydroxyl group is situated at about 3650 cm^{-1} . The band of H-bonded hydroxyl groups is situated at about 3540 cm^{-1} . From the area of the $(\nu+\delta)$ OH band at 4560 cm^{-1} (inset of figure 2), we have estimated the total concentration of Si-OH groups (both on the surface and in the wall) (Table 3, column 1), using the methodology described in reference [34]. In this way, there is no bias from a possible contribution of physisorbed water.

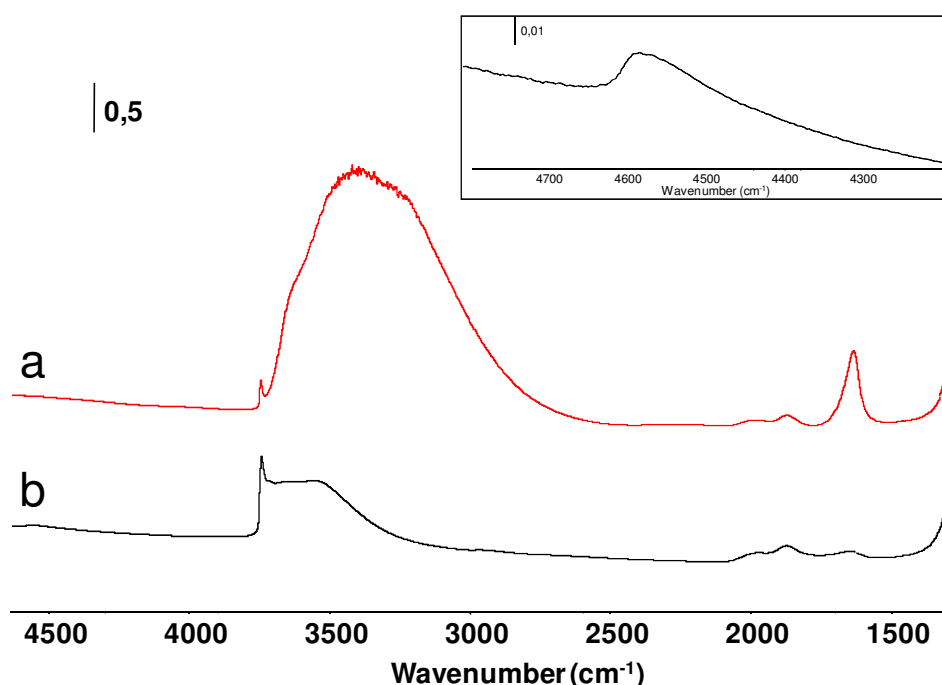


Figure 2: Infrared spectra of SBA-15 sample in the $1500\text{-}5500\text{ cm}^{-1}$ range. a) Spectrum recorded under atmosphere conditions. b) Spectrum recorded after degassing.

3.3 The various OH species according to MAS ^{29}Si NMR

The OH species were quantified using MAS ^{29}Si NMR and the NMR band was located using CP MAS ^1H ^{29}Si . It is well known that ^{29}Si MAS NMR is a sensitive technique to show the presence of different types of silicon sites in solids. In siliceous zeolite, silicon species are depicted as Q^4 if the silicon is surrounded with four $-\text{O}-\text{Si}$ groups, Q^3 if one $-\text{O}-\text{Si}$ group is replaced with one OH group,

etc... These species present a very different chemical shift. The CP MAS $\{^1\text{H}\}$ - ^{29}Si is a technique that highlights the presence of OH groups, which elucidates the ^{29}Si MAS spectrum. Just as it is the case with the in-situ IR measurements, solid state NMR is a bulk analysis tool. It measures both the silanols on the surface and in the walls of the materials.

3.3.1 The OH species for MCM and SBA materials

First the pure silica materials (MCM and SBA-type) are compared. Spectra obtained by direct polarization and by CP-MAS are presented in figure 3 A and B, respectively. Figure 4 depicts the NMR spectra for the silica materials with the Q^2 , Q^3 and Q^4 sites, as well as schematic explanation of these three species. It is interesting to see differences in intensity and width in the three Q^n peaks in the direct spectra (figure 3A) as well as in the cross polarized spectra (figure 3B). The amount of $\text{SiO}_2(\text{OH})_2$ (geminal silanol), SiO_3OH (single silanol) and SiO_4 species, respectively, are then estimated for all samples by using deconvolution, as presented in figure 3, and comparison with peak intensity in CPMAS.

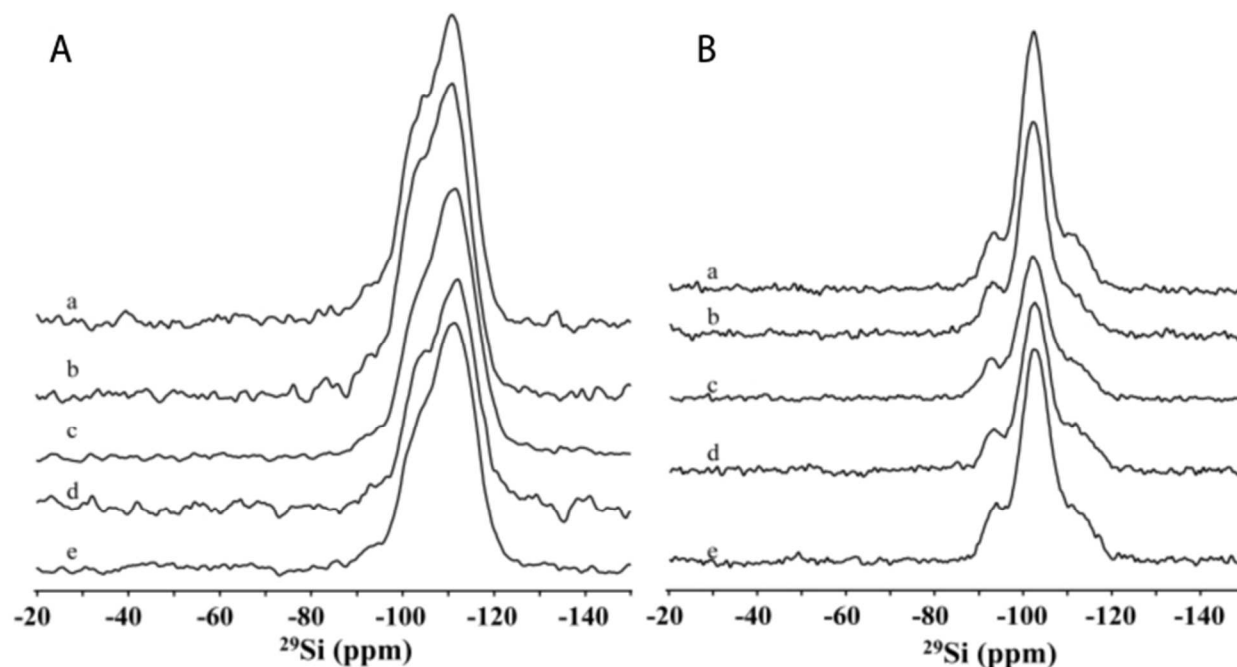


Figure 3: The ^{29}Si MAS NMR (A) and the CPMAS $\{^1\text{H}\}$ - ^{29}Si (B) spectrum for MCM-41HT (a), MCM-48 (b), MCM-41SD (c), SBA-15 (d) and SBA-16 (e).

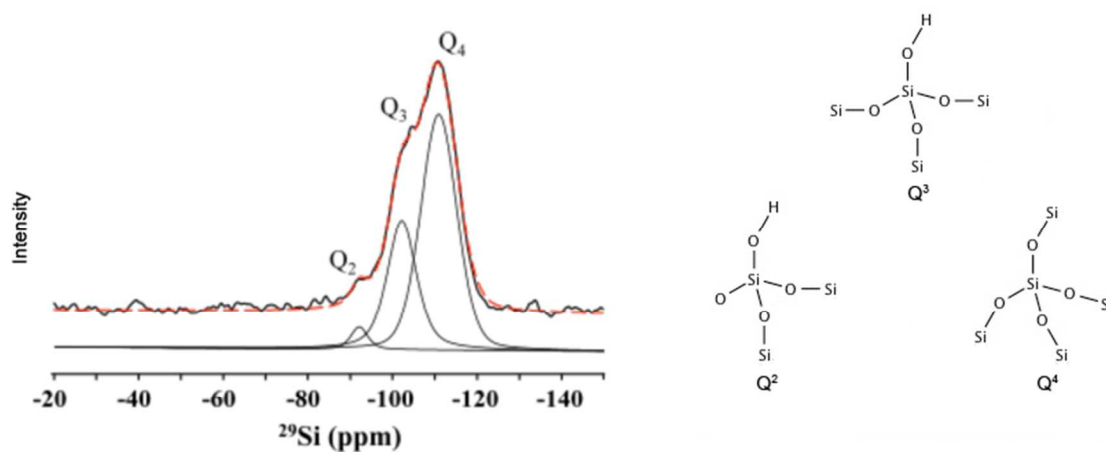


Figure 4: The allocation of the Q^2 , Q^3 and Q^4 site on the NMR spectra of the MCM and SBA materials.

From the integration of the three different peaks obtained in each sample it has been possible to estimate the relative amount of each species. The quantification results are then presented in table 3.

Table 3: The silanol number and the Q^2 , Q^3 and Q^4 species in the material.

	1	2	3	4	5	6	7
	Silanol content (IR)			SiO_3OH (%)	$SiO_2(OH)_2$ (%)	Total SiOH ratio	Condensation degree
Material	α_{OH} (mmol/g)	Q^3/Q^4	Q^2/Q^4	$Q^3/(Q^2+Q^3)$	$Q^2/(Q^2+Q^3)$	$(Q^2+Q^3)/(Q^2+Q^3+Q^4)$	$Q^4/(Q^2+Q^3+Q^4)$
SBA-15	3.5	0.30	0.04	88	12	0.25	0.75
SBA-16	8.3	0.52	0.02	96	4	0.35	0.65
MCM-41	3.6	0.62	0.04	94	6	0.40	0.60
MCM-48	5.2	0.67	0.04	94	6	0.42	0.58
MCM-41(SD)	3.2	0.35	0.01	97	3	0.26	0.74

Column 1 shows the silanol concentration acquired with infrared spectroscopy. This is the total silanol content, so both the surface silanols as the ones in the wall. A general trend visible in these

1 data is that thick walled materials (SBA type materials) exhibit a higher number of total silanol
2 groups. Columns 2 and 3 depict the Q³:Q⁴ and Q²:Q⁴ ratios of the various materials. The thin-
3 walled MCM materials exhibit a much higher percentage of surface silicon atoms, due to thinner
4 walls. A rough estimate of the percentage of surface silicon atoms is shown in the supplementary
5 information (table S1). They therefore also have a much higher percentage of Q³-sites than the
6 thick-walled SBA-type materials. Since silanol groups are preferentially at the surface it can be
7 understood that MCM materials exhibit a slightly higher Q³:Q⁴ ratio than SBA materials. Columns
8 4 and 5 depict the separate percentages of SiO₂(OH)₂ and SiO₃OH species respectively indicated as
9 geminal and single silanols. The total percentage of hydroxylated silicon atoms (SiO₂(OH)₂ +
10 SiO₃OH) is shown in column 6. The last column (7) is the complement of the total percentage of
11 hydroxylated silicon atoms and is designated as the condensation degree. The condensation
12 degree is larger for hydrothermally synthesized SBA materials in comparison with hydrothermal
13 MCM materials. Because the wall thickness of SBA materials is higher than MCM materials this
14 indicates that the total amount of hydroxylated silicon atoms lowers with the wall thickness.
15 Therefore it can be concluded that the main part of the silanol groups is situated at the pore
16 wall/air interface.

17 Remarkably the spray dried MCM-41 has a higher condensation degree than the other MCM-
18 type materials. This higher degree of condensation cannot be correlated to the wall thickness,
19 because this is comparable with the other MCM type materials. However, this can be explained by
20 the synthesis procedure. During the spray drying process, sol droplets are atomized and
21 evaporated at 220 °C. This is a much higher condensation temperature than for the hydrothermal
22 synthesis of MCM and SBA type materials, that typically does not exceed 110°C. Additionally the
23 ageing step usually applied to promote further condensation and reordering of the structure after
24 precipitation is not present in spray dried samples. This high temperature of spray drying
25 combined with the rapid and constant evaporation of the solvent and the ethanol produced by the

1 hydrolysis of the ethoxy functions of the silane, will eventually result in a higher degree of
2 condensation.
3
4
5
6

7 3.3.2 The OH-species for ethene PMOs 8 9

10
11
12 In comparison with the chemical shifts of the silicon atoms of pure silica materials in ^{29}Si MAS
13 NMR, a significant and distinct shift occurs for organosilica materials. Typically, the signals for the
14 silicon atoms with attached ethene bridges are located between -60 and -90 ppm.[45] The
15 spectrum and a schematic overview of the different T sites are depicted in figure 5. No Q-sites
16 were measured which indicates that no ethene bridges were broken during the synthesis of the
17 silica material.
18
19
20
21
22
23
24
25
26
27
28
29
30
31
32
33
34
35
36
37
38
39
40
41
42
43
44
45
46
47
48
49
50
51
52
53
54
55
56
57
58
59
60

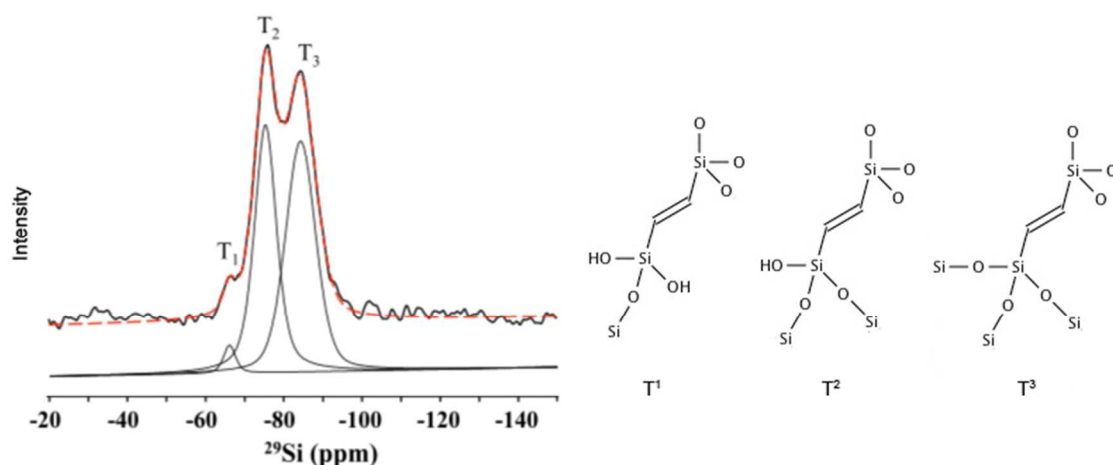
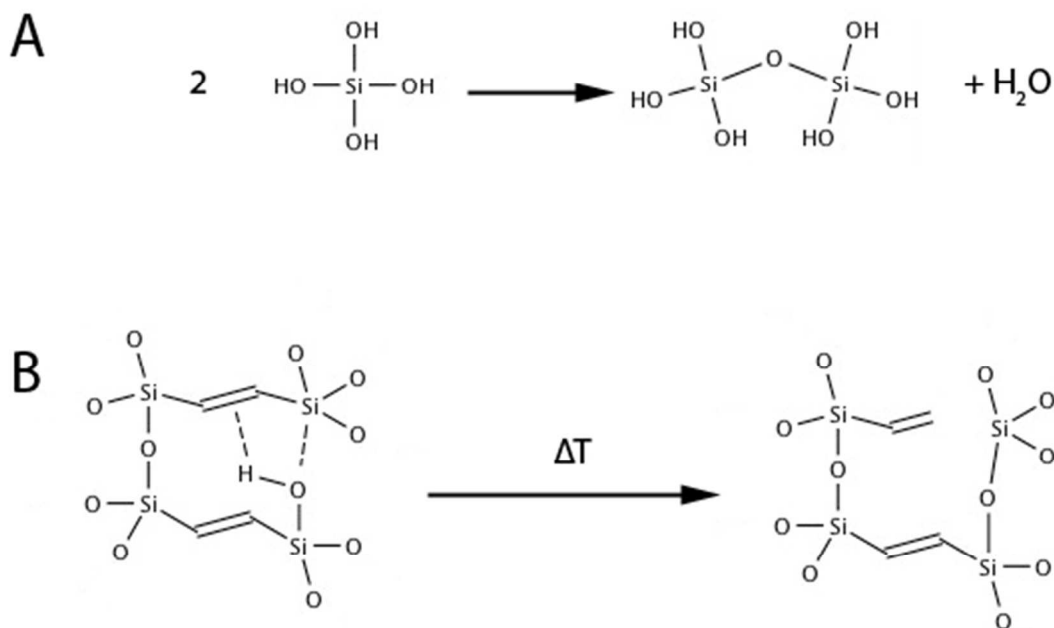


Figure 5: The allocation of the T¹, T² and T³ site on the NMR spectra of the PMO material.

Table 4 depicts the quantified silicon species from this spectrum. Column 1 repeats the total silanol number obtained with in-situ IR spectroscopy. Columns 2 and 3 show the T²:T³ and T¹:T³ ratios of the ethene PMO material. Columns 4 and 5 give the respective percentages of single (T²) and geminal (T¹) silanol groups. Column 6 depicts the total percentage of hydroxylated silicon atoms and column 7 is the complement of this value, designated as the degree of condensation.

1 When the total amount of OH species (columns 1 and 6) is compared to these on pure silica
2 materials (table 3: columns 1 and 6), there are more hydroxyl groups present in the organosilica
3 material. This is reflected in a much lower (below 50%) degree of condensation (column 7). Two
4 different mechanisms lead to these differences. First of all the polycondensation reaction of the
5 ethene bridged precursor molecule does not progress to completion because there are six
6 siloxane bridges to be formed per precursor molecule instead of the four of TEOS. (See the T³ sites
7 in Figure 5). This is sterically more difficult than the polycondensation reaction with TEOS, used
8 in the synthesis of MCM and SBA type materials. The second and probably the largest influence on
9 the degree of condensation, is the temperature of the post treatment. While pure silica materials
10 are calcined at 550°C, organosilicas are obviously not. The surfactant that acts as the porogen
11 inside the Periodic Mesoporous Organosilicas is typically extracted by Soxhlet extraction with
12 acetone or ethanol. [41] The materials are never exposed to temperatures above 120°C. When
13 PMOs are treated at temperatures above 200°C, the residual silanols will be further reduced by
14 interaction with the ethene bridge, via an autohydrophobisation reaction, as described by Ozin
15 [46] and Vercaemst [47]. These reactions can be shown as follows:
16
17
18
19
20
21
22
23
24
25
26
27
28
29
30
31
32
33
34
35
36
37
38
39
40
41
42
43
44
45
46
47
48
49
50
51
52
53
54
55
56
57
58
59
60



23 **Figure 6:** The polycondensation of silicates (A) and the autohydrophobisation illustrated for
24 ethene PMOs (B).
25
26
27

28 Finally, as the temperature reaches 300°C, the organic bridges will be destroyed.
29
30

31 **Table 4:** The silanol number and the T¹, T² and T³ species in the material.
32
33
34

	1	2	3	4	5	6	7
	Silanol number (IR)			SiO ₂ OH (%)	SiO ₁ (OH) ₂ (%)	Total SiOH ratio	Condensation degree
Material	α _{OH} (mmol/g)	T ² /T ³	T ¹ /T ³	T ² /(T ¹ +T ²)	T ¹ /(T ¹ +T ²)	(T ¹ +T ²)/(T ¹ +T ² +T ³)	T ³ /(T ¹ +T ² +T ³)
EthenePMO	16.9	1.16	0.06	95	5	0.55	0.45

35
36
37
38
39
40
41
42
43
44
45
46
47
48
49
50
51
52
53
54
55
56
57
58
59
60

3.4 Determination of the maximum loading of the probing molecules

The maximum loading of the materials was determined via the grafting procedure of three silanes that differ in carbon chain length. Through the accessible silanol groups, the probing molecules were anchored to the surface. The amount of probing molecules was quantified on the carbon amount determined with elemental analysis.

1 Table 6 depicts the loading capacity of the various (organo)silica materials for a trimethylsilyl
2 (C3), an octyldimethylsilyl (C8) and an octadecyldimethylsilyl (C18) group. The pore diameter has
3 been added for reference. From this table it can be observed that for the same reaction time the
4 amount of grafted groups drops with the length of the aliphatic chain. When the hydrothermally
5 synthesized pure silica materials are compared, the general tendency is that with smaller pores a
6 lower amount of groups are grafted on the surface (MCM vs SBA vs Nucleosil). The same tendency
7 has been shown as a function of the pore size of MCM materials by Waksburg et al.[48]
8
9

10 A first interesting observation can be made when SBA-15 is compared with SBA-16 and MCM-41
11 with MCM-48. The cubical pore systems (SBA-16 and MCM-48) systematically have a larger
12 amount of C18 groups anchored to the surface. This is due to the fact that a cubical pore system is
13 accessible from three dimensions while a hexagonal pore system just from one dimension.
14 Therefore it is clear that the inside of an SBA-16 and an MCM-48 particle can be reached more
15 easily and thus faster than the inside of an SBA-15 and MCM-41 particle. This easy access to the
16 whole of the pore system from multiple dimensions is the reason the carbon loading on cubic pore
17 systems is higher than the loading on hexagonal pore systems. The difference between the
18 hexagonal and the cubical system is higher for the SBA materials than for the MCM materials. A
19 possible explanation for this might be that in the case of SBA-16 some trapping of the C18 chains
20 into the pores occurs as SBA-16 has an Im3m cage like pore system. This would not happen in the
21 MCM-48 system because it does not have a central cage with smaller pore windows, but can be
22 described as a single sheet that winds through space following a gyroid surface.[49]
23
24
25
26
27
28
29
30
31
32
33
34
35
36
37
38
39
40
41
42
43
44
45
46
47

48 This theory is confirmed by Nucleosil where the amount of grafted groups per nm² is much
49 higher in comparison with the other materials. The Nucleosil material consists of perfect spheres
50 with large disordered pores (~ 30 nm). This much higher loading for Nucleosil confirms that the
51 grafting procedure for porous systems is strongly diffusion regulated. The influence of diffusion is
52
53
54
55
56
57
58
59
60

larger for the longer and more bulky grafting molecules than for the smaller ones and is larger for the hexagonal one-dimensional pore systems than for the cubic three-dimensional pore systems.

However when the molar amount of groups per weight unit (mmol/g) is considered it is immediately clear that the ordered mesoporous materials exhibit a much higher loading than the commercial Nucleosil material.

Table 5: Overview of the micropore volume ($V_{p,\mu,t\text{-plot}}$) and surface area ($SA_{\mu,t\text{-plot}}$) by t-plot analysis; the mesopore volume ($V_{p,m,BJH}$) and surface area ($SA_{m,BJH}$) by BJH analysis; the total pore volume ($V_{p,0.95}$) taken at $P/P^\circ = 0.95$ and surface area (SA_{BET}) by BET analysis of SBA-15, SBA-16 and ethene PMO.

Material	SA_{BET}	$SA_{\mu,t\text{-plot}}$	$SA_{m,BJH}$	$V_{p,0.95}$	$V_{p,\mu,t\text{-plot}}$	$V_{p,m,BJH}$
	m ² /g	m ² /g	m ² /g	cm ³ /g	cm ³ /g	cm ³ /g
SBA-15	655	460	429	0.84	0.07	0.74
SBA-16	738	469	398	0.63	0.11	0.47
EthenePMO	923	649	598	0.99	0.07	0.87

A second observation is the higher surface silanol loading of the SBA-type materials, compared to the MCM-type materials, regardless of the mesoscopic structure. This is particularly evident for the silanols that are accessible to the smallest silanes (C3, HMDS). This fact finds its origin in the synthesis methods. The SBA-type materials are synthesized by Pluronic surfactants, which are ethyleneoxide/propyleneoxide triblock copolymers. The ethenylene oxide side chains create microporous perforations in the SBA-walls. The SBA-type materials (and the PMO material that was also synthesized using the Pluronic 123 surfactant) therefore have an important fraction of micropores.[50] Table 5 shows an overview of the micropore volume and micropore surface area of these materials. It is clear that these micropores contribute very significantly to the total pore area and lie at the origin of the higher concentration of surface

accessible silanols. Note that the difference between the BET surface area and the sum of the micropore and the mesopore surface area based on the t-plot and BJH models respectively lies within the typical error of analysis.

Table 6: The loading capacity for relevant chromatographic groups for various ordered mesoporous (organo)silica materials.

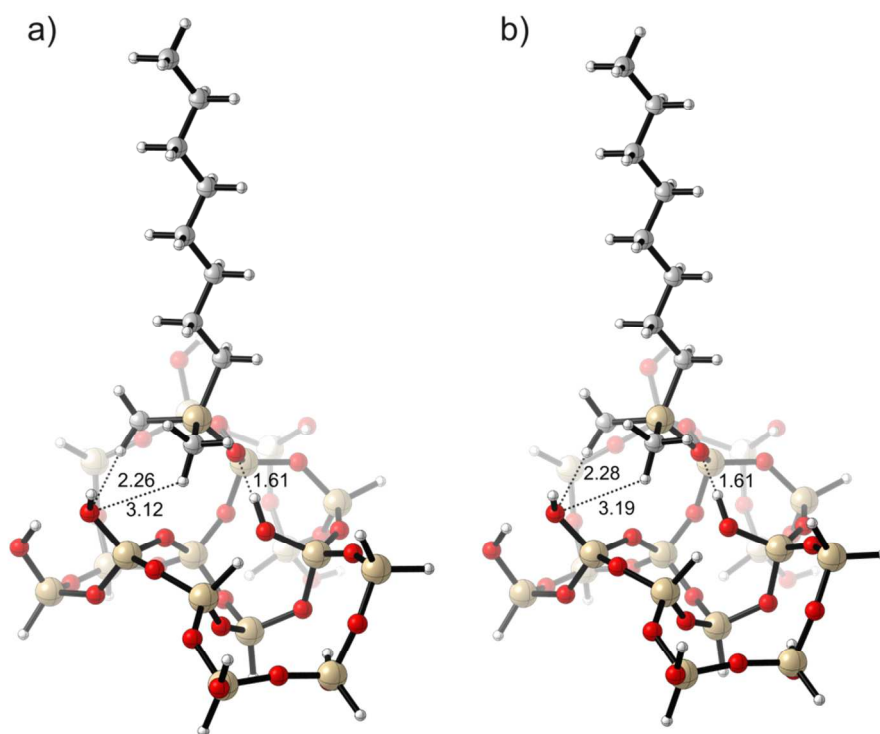
Material	Pore size	C3		C8		C18	
		nm	mmol/g	groups/nm ²	mmol/g	groups/nm ²	mmol/g
SBA-15	6.9	1.8	1.7	0.7	0.7	0.1	0.1
SBA-16	6.2	2.3	1.9	0.8	0.7	0.5	0.4
MCM-41	2.9	2.2	1.2	0.9	0.5	0.4	0.2
MCM-48	2.8	2.5	1.2	1.2	0.6	0.5	0.3
MCM-41(SD)	2.9	1.9	1.6	1.0	0.8	0.3	0.3
EthenePMO	6.2	1.1	0.7	0.8	0.5	0.4	0.2
Nucleosil	~ 30	0.4	2.8	0.5	3.3	0.3	1.9

3.5 Computational considerations

To get a better view on the behavior of silane groups on the silica surface, theoretical calculations were performed to determine the geometry of a carbon chain substituent. All results were obtained with the gaussian09 software package [51] using a B3LYP functional [52, 53] with a 3-21G Pople basis set. Since the primary focus was set on determining geometries this level of theory was chosen.

First, a random silica slab was made with approximately 5.3 hydroxyl groups per nm². This model is designed to represent an amorphous silica surface, thus a random cluster was built with the required silanol-density. To calculate the density the total number of hydroxyl groups was

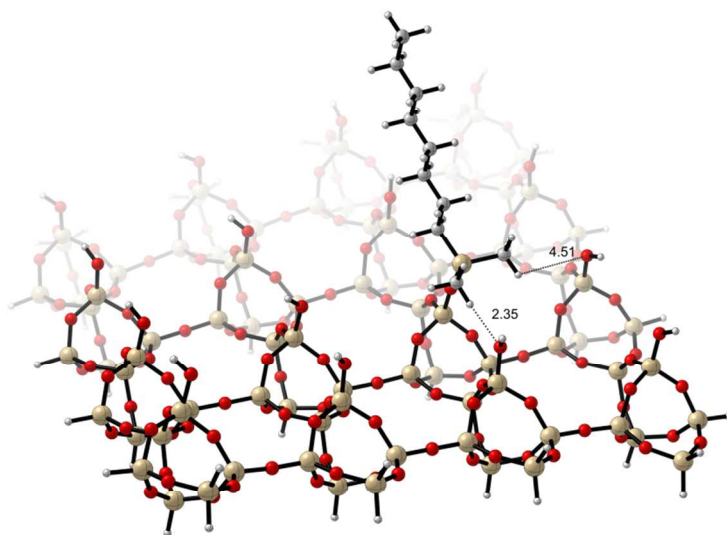
1 divided by the exposed surface of the cluster, hydroxyl groups at the edge are only counted as half
2 since they are also part of neighboring clusters. The proposed approach was chosen since there
3 are no surface models available for silicas with this high silanol loading. The edges of the slab are
4 saturated with hydrogen atoms, which were unrestricted during the optimization. One of the
5 hydroxyl groups was exchanged with a C8 silane group. Geometry optimizations with the
6 described methodology show the tail is oriented to minimize the interactions with the surface.
7 This is as expected, since the apolar tail cannot interact with the polar surface (Figure 7).
8
9
10
11
12
13
14
15
16



43 **Figure 7:** Random silica surface with 5.3 hydroxyl group per nm² and one C8 silane substituent.
44 This silane blocks two neighboring silanol groups. Figure a) is without an implicit solvent model,
45 b) is the same starting geometry optimized with such a model. The differences are minimal.
46
47
48
49

50 Similar calculations, where an implicit solvent model (IEFPCM[54]) was added, characterized by
51 the dielectric constant of toluene, gave comparable results. The geometrical results show that only
52 the -Si(CH₃)₂- moiety imposes a limit on the number of possible substituents per surface area.
53 From the result it can be seen that the -Si(CH₃)₂- moiety blocks at least two extra hydroxyl
54
55
56
57
58
59
60

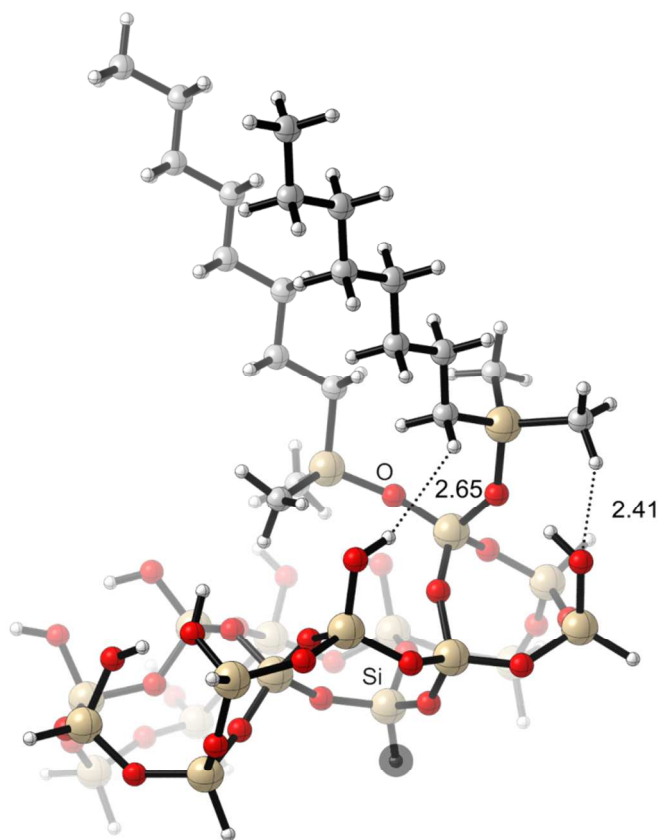
1 groups. Since those groups can also be overlapped by another silane group from a more distant
2 position, they are only counted as half. So it can be concluded that, on this dense cluster, at least
3 position, they are only counted as half. So it can be concluded that, on this dense cluster, at least
4 two groups are needed to accommodate the substituent leading to a maximum possible loading of
5 2.65 groups per nm². On a less dense surface with about 2.5 hydroxyl groups per nm² there are no
6 neighboring positions blocked (Figure 8).
7
8
9
10
11



12
13
14
15
16
17
18
19
20
21
22
23
24
25
26
27
28
29
30
31
32
33
Figure 8: Surface model with about 2.5 hydroxyl groups per nm² the surface is based on an
34 ordered silica slab. The silane group is close to a neighboring hydroxyl group, but since the
35 surface is more open this does not block the site. As an upper bound, on this type of surface it is
36 possible to have 2.5 silane substituents per nm². However, when the surface is almost full, the
37 close interaction (2.35Å) will fully shield one of the hydroxyl groups and the theoretical maximum
38 will never be reached.
39
40
41
42
43
44
45
46
47

48
49 This means the theoretical density in this case is 2.5 groups per nm². On average, 2.5 groups per
50 nm² is the theoretical maximal loading on a silica surface with only single silanols present, this is
51 close to the value that can be estimated from the kinetic diameter of the silane and that was
52 reported previously by Van Der Voort. [55]
53
54
55
56
57
58
59
60

1 To assess the influence of geminal silanols a slight modification on the random surface was
2 made, an extra hydroxyl group was added on a silicon atom and one Si-O-Si bond on that atom
3 was broken. The other silicon atom was saturated by hydrogen. With this approach the surface
4 contains a single geminal group. Two silane groups were placed on this site and after geometry
5 optimization it appeared that at least two extra silanol groups were blocked by this. (Figure 9).
6
7
8
9
10
11
12
13
14
15
16
17
18
19
20
21
22
23
24
25
26
27
28
29
30
31
32
33
34
35
36
37
38
39
40
41
42
43
44
45
46
47



48 **Figure 9:** The original cluster is modified to incorporate a geminal silanol, the Si-O bond between
49 the atoms explicitly named on the figure was broken and the marked hydrogen atom was added
50 for saturation, a second silane group was then added to the free oxygen. With two silane groups
51 on a geminal silanol two other silanol groups are blocked. This allows a more efficient stacking of
52 the substituents.
53
54
55
56
57
58
59
60

For the same reason as before they only count as half. With the extra hydroxyl group from the geminal silanol, the surface silanol density is 6.7 groups per nm² (the surface area remains unchanged but an extra hydroxyl group is added). This means that when one extra hydroxyl group is blocked by the silane moiety, the density of substituents on the surface can be calculated as:

$$\frac{2 \text{ silane groups} \cdot 6.7 \text{ gr/nm}^2}{3 \text{ hydroxy groups}} = 4.5 \text{ gr/nm}^2$$

A fully hydroxylated silica surface (single silanol groups) can have maximum of 4.6 ± 0.5 groups per nm². This means that roughly only half of the single silanol groups is sterically available for grafting which coincides with previous reports on that matter.[9]

In Table 7 we summarize the total silanol number, differentiated as total, geminal and single silanols and the silanol that are accessible for the small HMDS molecule, expressed in mmol per gram and in groups per nm².

Table 7: The bulk silanol number, the amount of single and geminal silanols and the surface silanol groups, depicted with the pore diameter (d_p) and pore wall (h).

	1	2	3	4	5	6	7
Material	α _{OH,bulk} (mmol/g)	α _{OH,single,bulk} (mmol/g)	α _{OH,geminal,bulk} (mmol/g)	α _{OH,surface} (mmol/g)	α _{OH,surface} (gr/nm ²)	h (nm)	d _p (nm)
SBA-15	3.5	3.1	0.4	1.9	1.7	4.2	6.9
SBA-16	8.3	8.0	0.4	2.3	1.9	6.4	6.2
MCM-41HT	3.6	3.4	0.2	2.3	1.2	1.1	2.9
MCM-48	5.2	4.9	0.2	2.6	1.2	1.0	2.8
MCM-41SD	3.2	3.1	0.1	1.9	1.6	1.2	2.9
EthenePMO	16.9	14.3	2.6	1.1	0.7	3.1	6.2

1 The amount of single and geminal silanols (columns 2 and 3 in table 7) are calculated by
2 multiplying the relative amount of silanols with the total number of OH-groups determined by IR
3 spectroscopy (i.e. $\alpha_{OH} \times (Q^3/(Q^2+Q^3)) = \alpha_{OH,single}$). This gives the absolute amount single and geminal
4 silanols, irrespective of their location. They could be on the pore wall or in the bulk silica.
5
6
7
8

9
10 Column 4 in table 7 then shows the silanols that were available to the small HMDS (C3 silane).
11 Because none of these values exceed the theoretical maximum values they can be considered as
12 the “surface” or “reachable” silanols.
13
14
15

16 17 18 19 4 Conclusion 20 21 22 23

24 We have established that the amount of silane groups (expressed as groups per nm²) that can be
25 grafted on the surface of ordered mesoporous silicas (MCM-41, MCM-48, SBA-15, SBA-16) is much
26 smaller than on the surface of the commercial materials, which are typically used as a packing
27 material for HPLC columns. The main reason for this is that the grafting reaction is strongly
28 diffusion limited, as the surface area of these materials is basically internal surface area.
29
30
31
32
33
34
35

36 For the mesoporous silicas, it can be concluded that the amount of surface silanols is larger for
37 the micropore containing SBA-type materials than for the non microporous MCM-type materials.
38 The amount of internal silanol groups is proportional, however not linearly, to the wall thickness.
39 Silica materials with thicker walls (SBA-15, SBA-16 and ethene PMO) also have more total silanol
40 groups than the thin walled MCM-materials. In general, for the thick walled mesoporous silicas,
41 one should keep in mind that up to 70% of the silanols is unreachable for a small silane.
42
43
44
45
46
47
48
49

50 Spray dried MCM-41 exhibits a more condensed silica structure due to the higher synthesis
51 temperature. The PMO material (ethene PMO) on the other hand exhibits a lower condensation
52 degree. This can be attributed to the different condensation behavior of $(EtO)_3Si-CH=CH-Si(OEt)_3$
53 compared to $Si(OEt)_4$ and to the absence of a high temperature calcinations procedure.
54
55
56
57
58
59
60

1
2
3 Acknowledgements:
4
5

6
7 M.I. acknowledges the IWT-Flanders (Agentschap voor Innovatie door Wetenschap en
8
9 Technologie) grant nr. IWT/SB/71325 for financial support. T.B. is indebted to Ghent University,
10
11 GOA-grant, project number 01G00710 and the European Research Council (FP7(2007-2013) ERC
12
13 grant nr. 240483). Computational resources and services were provided by Ghent University.
14
15
16
17
18
19
20
21
22
23
24
25
26
27
28
29
30
31
32
33
34
35
36
37
38
39
40
41
42
43
44
45
46
47
48
49
50
51
52
53
54
55
56
57
58
59
60

References

- 1
2
3
4 [1] Bartle, K.D.; Carney, R.D.; Cavazza, A.; Cikalo, M.G.; Myers, P.; Robson, M.M.; Roulin,
5
6 S.C.P.; Sealey, K. J. *Chrom. A* **2000**, *892*, 279.
7
8
9 [2] Sindorf, D.; Maciel, G. J. *Am. Chem. Soc.* **1983**, *105*, 1487.
10
11
12 [3] Kratochvila, J.; Salajka, Z.; Kazda, A.; Kadlc, Z.; Soucek, J.; Georghiu, M. *Journal of*
13
14 *Non-crystalline Solids* **1990**, *116*, 93.
15
16
17
18 [4] Kellum, G.; Smith, R. *Anal. Chem.* **1967**, *39*, 341
19
20
21 [5] Zhuravlev, L. *Colloids and Surfaces A-Physicochemical and Engineering Aspects*
22
23 **1993**, *74*, 71.
24
25
26
27 [6] Zhuravlev, L. *Langmuir* **1987**, *3*, 316.
28
29
30 [7] Zhuravlev, L. *Colloids and Surfaces A-Physicochemical and Engineering Aspects*
31
32 **2000**, *173*, 1.
33
34
35
36 [8] Nawrocki, J. *Journal of Chromatography A* **1997**, *779*, 29.
37
38
39 [9] Vansant, E.; Van Der Voort, P. ; Vrancken, K. *Characterization and Chemical*
40
41 *Modification of the Silica Surface; Studies in Surface Science and Catalysis; Elsevier Science BV,*
42
43 **1995**; Vol. 93.
44
45
46
47 [10] Ek, S.; Root, A.; Peussa, M.; Hiinistö, L.; *Thermochim. Acta*, **2001**, *379*, 201.
48
49
50 [11] McCool, B.; Murphy, L.; Tripp, C.P.; *J. Colloid Interf. Sci.*, **2006**, *295*, 294.
51
52
53
54 [12] Zholobenko, V.L.; Plant, D.; Evans, A.J.; Holmes, S.M.; *Micropor. Mesopor. Mater.*,
55
56 **2001**, *44-45*, 793.
57
58
59
60

- 1 [13] Léonardelli, S.; Facchini, L.; Fretigny, C.; Touyne, P.; Legrand, A.P.; J. Am. Chem. Soc.
2
3 **1992**, *114*, 6412.
4
5
6 [14] Liu, C.C.; Maciel, G.E.; J. Am. Chem. Soc., **1996**, *118*, 5103.
7
8
9 [15] Delitala, C.; Cadoni, E.; Delpiano, D.; Meloni, D.; Alba, M.D.; Becerro, A.I.; Ferino, I.,
10
11 Micropor. Mesopor. Mater. **2009**, *118*, 11.
12
13
14 [16] Sindorf, D.W.; Maciel, G.E.; J. Am. Chem. Soc., **1983**, *105*, 3767.
15
16
17
18 [17] Park, D.; Nishiyama, N.; Egashina, Y.; Ueyama, K.; Ind. Eng. Chem. Res. **2001**, *40*,
19
20 6105.
21
22
23 [18] Knözigner, H.; Schuster, P.; Zundel, G.; Sandorfy, C.; The Hydrogen Bond, vol 3,
24
25 North-Holland, Amsterdam, **1979**, p1263.
26
27
28
29 [19] Kruk, M.; Antochshuk, V.; Matos, J.; Mercuri, L.; Jaroniec, M.; J. Am. Chem. Soc. **2002**,
30
31 *124*, 768.
32
33
34 [20] Hansen, E.; Schmidt, R.; Stöcker, M.; Akporiaye, D.; J. Phys. Chem., **1995**, *99*, 4148.
35
36
37
38 [21] Grünberg, B.; Emmler, T.; Gedat, E.; Shendrovich, I.; Findenegg, G.H.; Limbach, H.;
39
40 Buntkowsky, G.; Chem. Eur. J., **2004**, *10*, 5689.
41
42
43 [22] Lebret, A.; Lelong, G.; Mason, P.; Saboungi, M.; Brady, J.; Food Biophysics, **2011**, *6*,
44
45 233.
46
47
48 [23] Shenderovich, I.; Buntkowsky, A.; Schreiber, A.; Gedat, E.; Sharif, S.; Albrecht, J.;
49
50 Golubev, N.; Findenegg, G.; Limbach, H.; J. Phys. Chem. B, **2003**, *107*, 11924.
51
52
53 [24] Pizzanelli, S.; Kababya, S.; Frydman, V.; Landau, M.; Vega, S.; J. Phys. Chem. B, **2005**,
54
55 *109*, 1997.
56
57
58
59
60

- 1
2
3
4
5
6
7
8
9
10
11
12
13
14
15
16
17
18
19
20
21
22
23
24
25
26
27
28
29
30
31
32
33
34
35
36
37
38
39
40
41
42
43
44
45
46
47
48
49
50
51
52
53
54
55
56
57
58
59
60
- [25] Landmesser, H.; Kosslick, H.; Fricke, R.; *Solid State Ionics*, **1997**, *101-103*, 271.
- [26] Kocherbitov, V.; Alfredsson, V.; *J. Phys. Chem. C*, **2007**, *111*, 12906.
- [27] Cauvel, A.; Brunel, F.; DiRenzo, F.; Garrone, E.; Fubini, B.; *Langmuir*, **1997**, *13*, 2773.
- [28] Blin, J.; Carteret, C.; *J. Phys Chem. C*, **2007**, *111*, 2773.
- [29] Sutra, P.; Fajula, F.; Brunel, D.; Lentz, P.; Daelen, P.; Nagy, J.; *Colloids Surf. A*, **1999**, *158*, 21.
- [30] Zhao, X.; Lu, G.; Whittaker, A.; Millar, G.; Zhu, H.; *J. Phys. Chem. B*, **1997**, *101*, 6525.
- [31] Llewellyn, P.; Schuth, F.; Grillet, Y.; Rouquerol, F.; Unger, K.; *Langmuir*, **1995**, *11*, 574.
- [32] Trebosc, J.; Wiench, J.; Huh, S.; Lin, U.; Prusky, M.; *J. Am. Chem. Soc.*, **2005**, *127*, 3057.
- [33] Shenderovitch, I.; Maudu, D.; Akcakayiran, G.; Buntkowsky, G.; Limbach, H.; Findenegg, G.; *J. Phys. Chem. B*, **2007**, *111*, 12088.
- [34] Gallas, J.-P.; Goupil, J.-M.; Vimont, A.; Lavalley, J.-C.; Gil, B.; Gilson, J.-P.; Miserque, O. *Langmuir* **2009**, *25*, 5825.
- [35] Zhao, D. Y.; Huo, Q. S.; Feng, J. L.; Chmelka, B. F.; Stucky, G. D. *J. Am. Chem. Soc.* **1998**, *120*, 6024.
- [36] Stevens, W. J. J.; Mertens, M.; Mullens, S.; Thijs, N.; Van Tendeloo, G.; Cool, P.; Vansant, E. F. *Micropor. Mesopor. Mater.* **2006**, *93*, 119.
- [37] Beck, J. S.; Vartuli, J. C.; Roth, W. J.; Leonowicz, M. E.; Kresge, C. T.; Schmitt, K. D.; Chu, C. T. W.; Olson, D. H.; Sheppard, E. W.; Mc-Cullen, S. B.; Higgins, J. B.; Schlenker, J. L. *J. Am. Chem. Soc.* **1992**, *114*, 10834.

- 1 [38] Collart, O.; Van Der Voort, P.; Vansant, E.; Desplantier, D.; Galarneau, A.; Di Renzo, F.;
2 Fajula, F. J. *Phys.Chem. B* **2001**, *105*, 12771.
3
4
5 [39] Ide, M.; Wallaert, E.; Van Driessche, I.; Lynen, F.; Sandra, P.; Van Der Voort, P.
6
7
8
9
10
11 [40] Goethals, F.; Vercaemst, C.; Cloet, V.; Hoste, S.; Van Der Voort, P.; Van Driessche, I.
12
13
14
15
16
17 [41] Vercaemst, C.; Ide, M.; Allaert, B.; Ledoux, N.; Verpoort, F.; Van Der Voort, P.;
18
19
20
21
22
23 [42] Kruk, M.; Jaroniec, M.; Sayari, A. *Chem.Mater.* **1999**, *11*, 492.
24
25
26 [43] Ravikovitch, P.; Neimark, A. *Langmuir* **2000**, *16*, 2419.
27
28
29 [44] Ravikovitch, P.; Neimark, A. *Langmuir* **2001**, *18*, 911.
30
31
32
33 [45] Vercaemst, C.; Ide, M.; Wiper, P.; Jones, J.; Khimyak, Y.; Verpoort, F.; Van Der Voort,
34
35
36
37
38
39 [46] Asefa, T.; MacLachlan, M.; Grondey, H.; Coombs, N.; Ozin, G.; *Angewandte Chemie Int.*
40
41
42
43
44 [47] Van Der Voort, P.; Vercaemst, C.; Schaubroeck, D.; Verpoort, F.; *Phys.Chem. Chem.*
45
46
47
48
49 [48] Waksburg, A.; Nguyen, M.-H. T.; Chaffee, A. L.; Kidder, M. K.; Buchanan, A. C., III;
50
51
52
53
54
55 [49] Anderson, M.; *Zeolites* **1997**, *19*, 220.
56
57
58
59 [50] Kruk, M.; Jaroniec, M.; Hyun, C.; Ryoo, R.; *Chem. Mater.* **2000**, *12*, 1961.
60

1 [51] M. J. Frisch, G. W. Trucks, H. B. Schlegel, G. E. Scuseria, M. A. Robb, J. R. Cheeseman, G.
2 Scalmani, V. Barone, B. Mennucci, G. A. Petersson, H. Nakatsuji, M. Caricato, X. Li, H. P. Hratchian, A.
3 F. Izmaylov, J. Bloino, G. Zheng, J. L. Sonnenberg, M. Hada, M. Ehara, K. Toyota, R. Fukuda, J.
4 Hasegawa, M. Ishida, T. Nakajima, Y. Honda, O. Kitao, H. Nakai, T. Vreven, J. A. Montgomery Jr., J. E.
5 Peralta, F. Ogliaro, M. Bearpark, J. J. Heyd, E. Brothers, K. N. Kudin, V. N. Staroverov, R. Kobayashi, J.
6 Normand, K. Raghavachari, A. Rendell, J. C. Burant, S. S. Iyengar, J. Tomasi, M. Cossi, N. Rega, J. M.
7 Millam, M. Klene, J. E. Knox, J. B. Cross, V. Bakken, C. Adamo, J. Jaramillo, R. Gomperts, R. E.
8 Stratmann, O. Yazyev, A. J. Austin, R. Cammi, C. Pomelli, J. W. Ochterski, R. L. Martin, K. Morokuma,
9 V. G. Zakrzewski, G. A. Voth, P. Salvador, J. J. Dannenberg, S. Dapprich, A. D. Daniels, O. Farkas, J. B.
10 Foresman, J. V. Ortiz, J. Cioslowski, D. J. Fox, Revision A.02, Gaussian, Inc., Wallingford CT ed.,
11 **2009**.

12 [52] A. D. Becke, J. Chem. Phys. **1993**, *98*, 5648.

13 [53] C. T. Lee, W. T. Yang, R. G. Parr, Phys. Rev. B **1988**, *37*, 785.

14 [54] E. Cancès, B. Mennucci, J. Tomasi, J. Chem. Phys. **1997**, *107*, 3032.

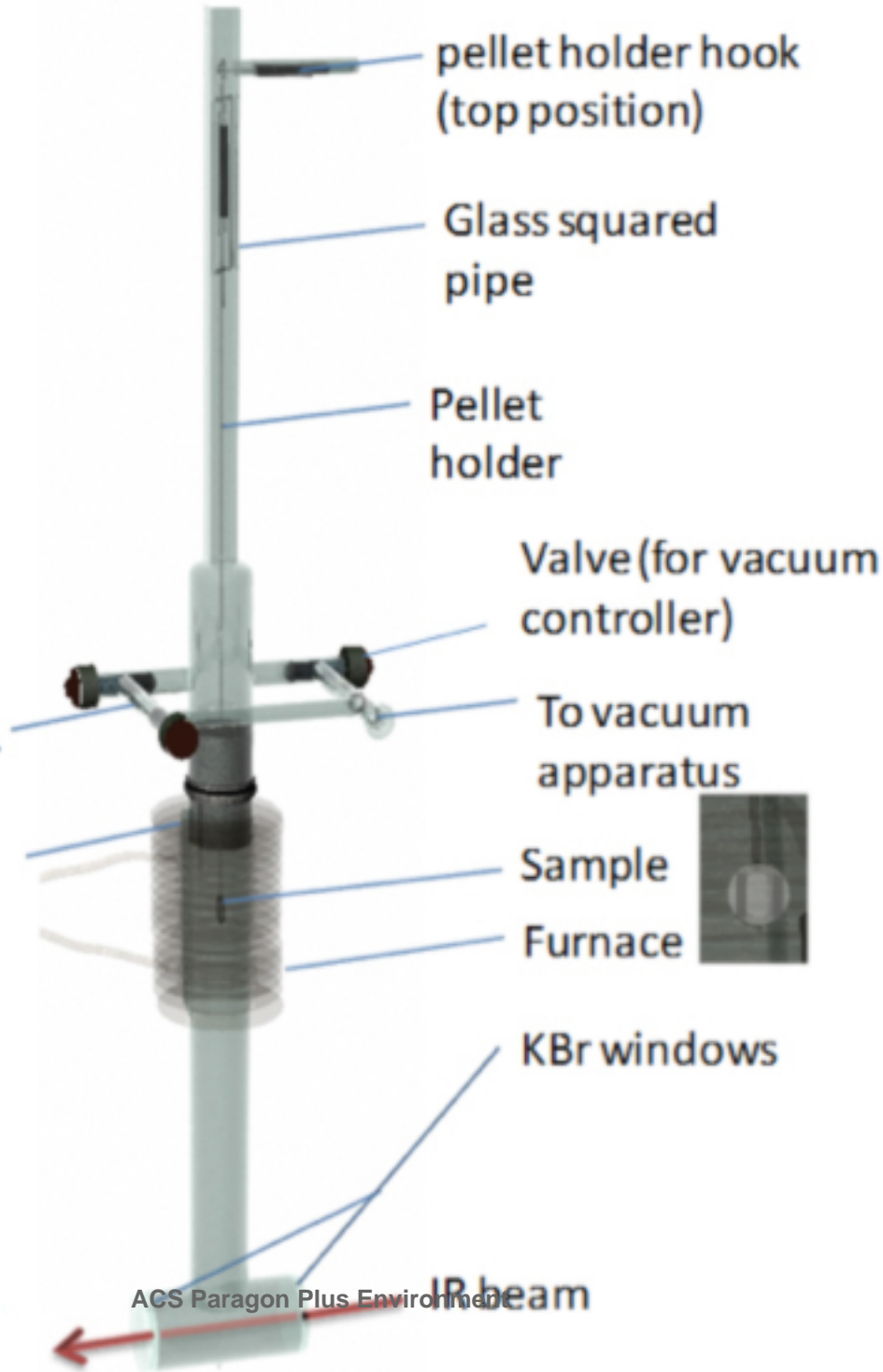
15 [55] Van Der Voort, P.; Vercauteren, S.; Peeters, K.; Vansant, E.; J. Colloid. Interface Sci.,
16 **1993**, *157*, 518.

17 [56] Iler, R. The Chemistry of Silica; **1979**.

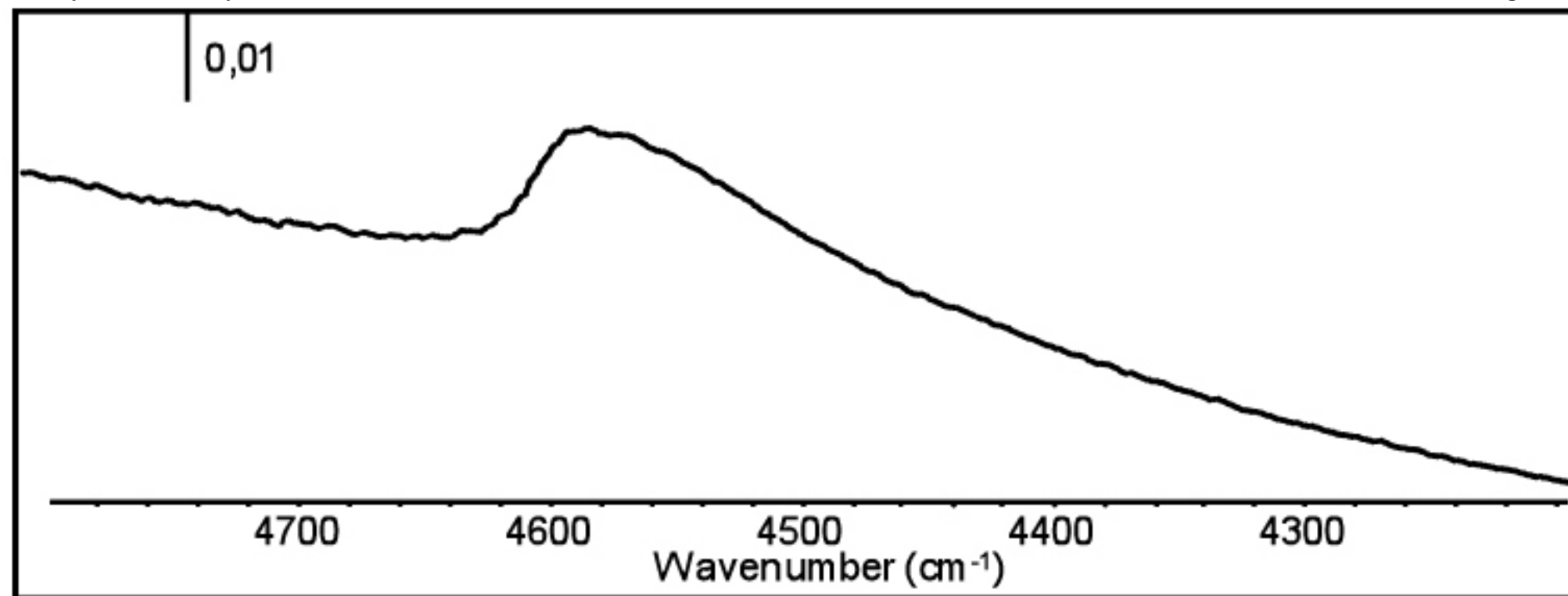
18 [57] Huo, O.; Magolese, D.I.; Ciesla, U.; Feng, P.; Gier, T.E.; Sieger, P.; Leon, R.; Petroff, P.M.;
19 Schüth, F.; Stucky, G.D.; Nature **1994**, *368*, 317.

20 [58] Hoffmann, F.; Cornelius, M.; Morell, J.; Fröba, M.; Angewandte Chemie Int. Ed., **2006**,
21 *45*, 3216.

1
2
3
4
5
6
7
8
9
10
11
12
13
14
15
16
17
18
19
20
21
22
23
24
25
26
27
28
29
30
31
32
33
34
35
36
37
38
39
40
41
42
43
44
45
46
47



| 0,5

**a****b**

4500

4000

3500

3000

2500

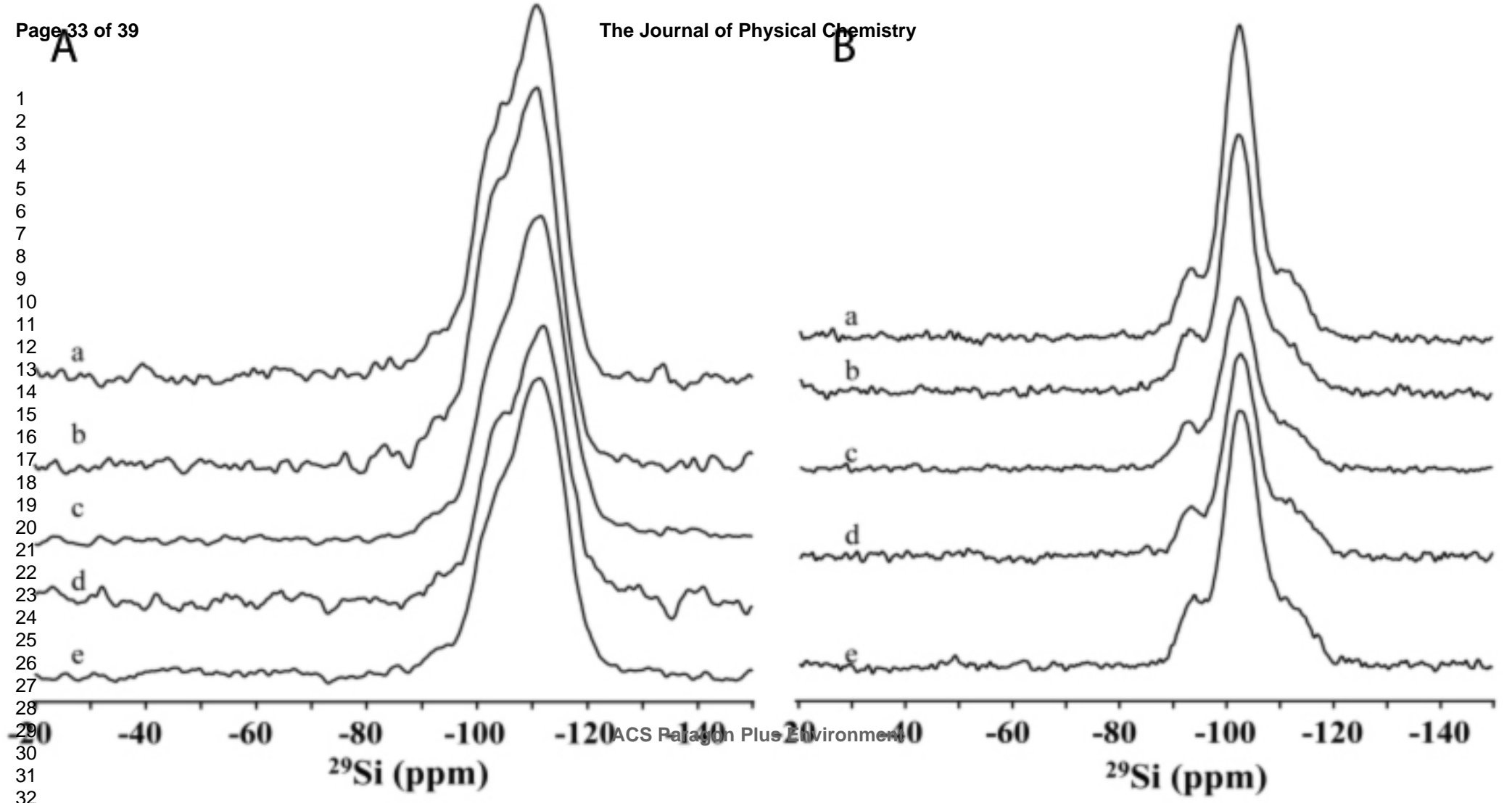
2000

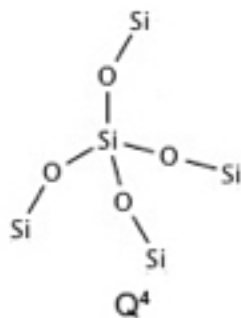
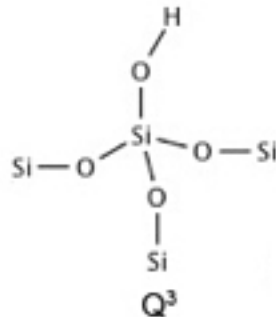
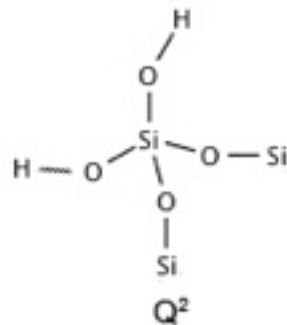
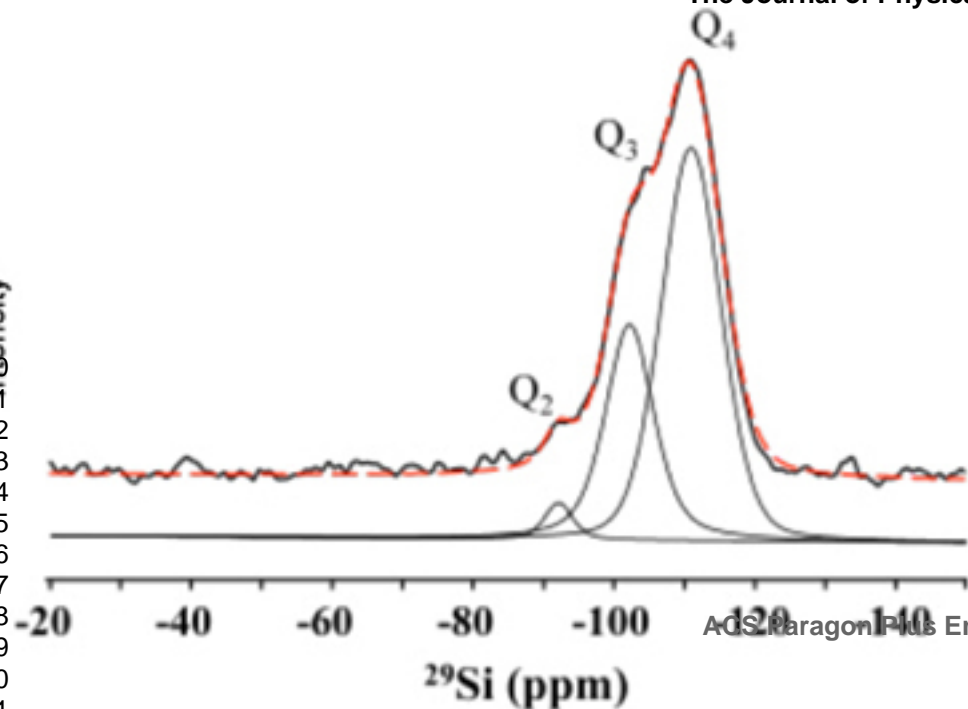
1500

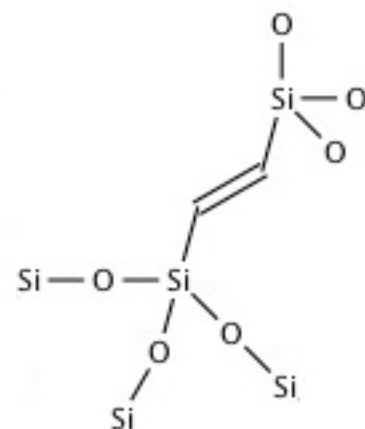
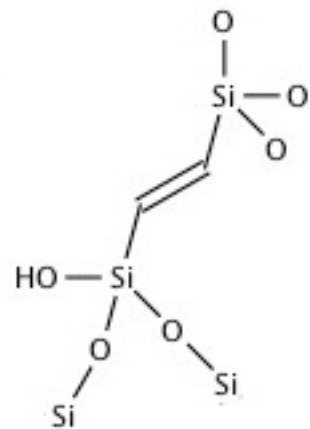
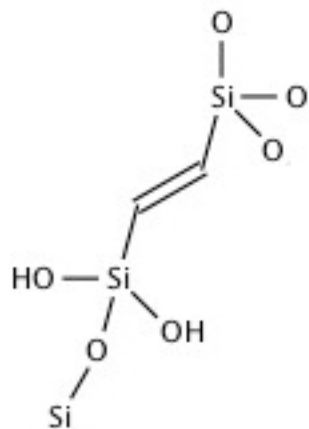
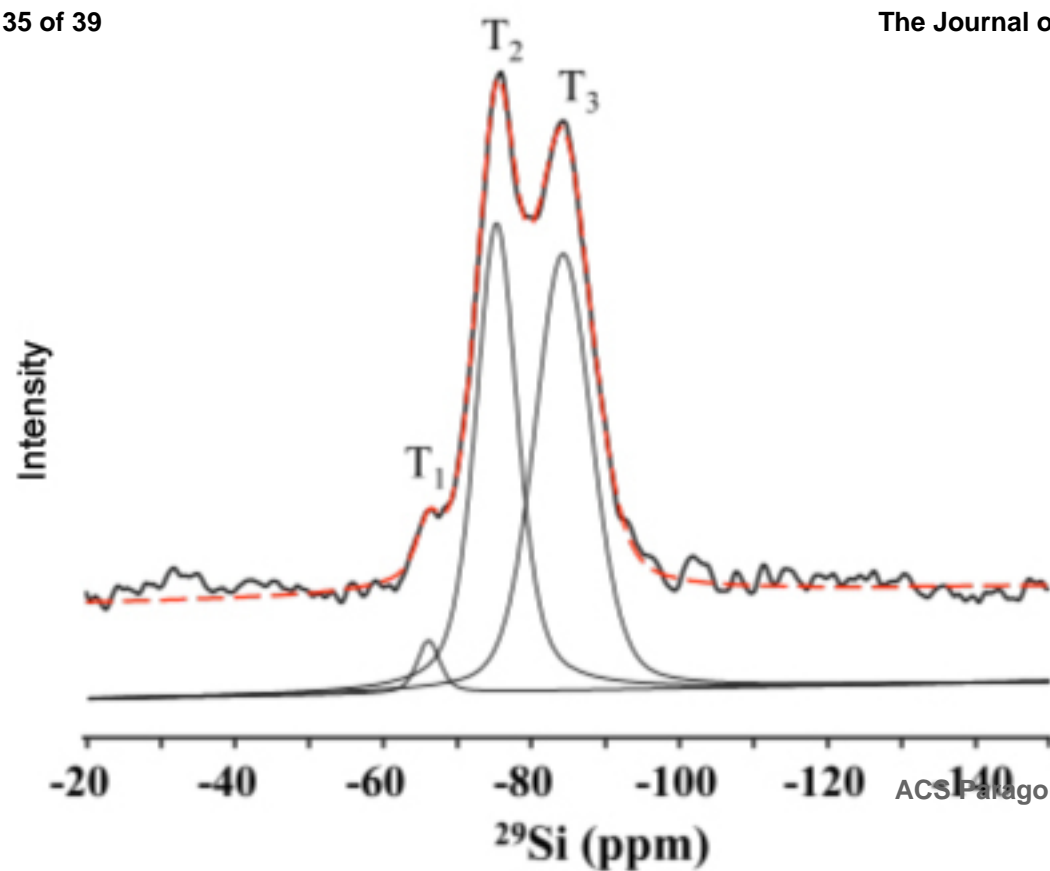
Wavenumber (cm^{-1})

A

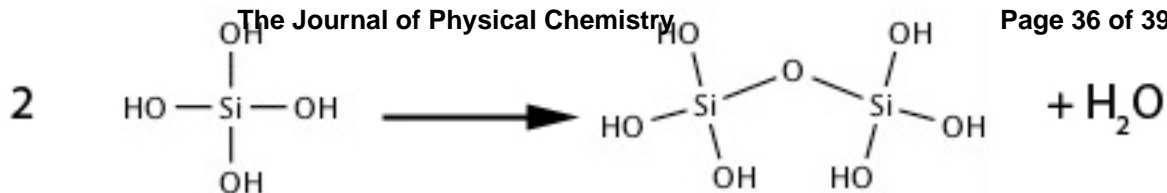
B

1
2
3
4
5
6
7
8
9
10
11
12
13
14
15
16
17
18
19
20
21
22
23
24
25
26
27
28
29
30
31
32

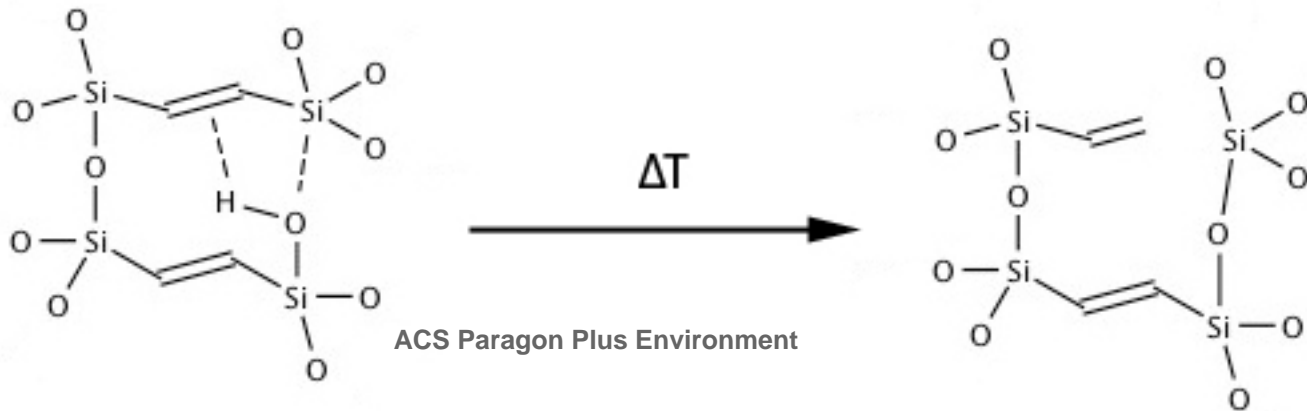
1
2
3
4
5
6
7
8
9
10
11
12
13
14
15
16
17
18
19
20
21



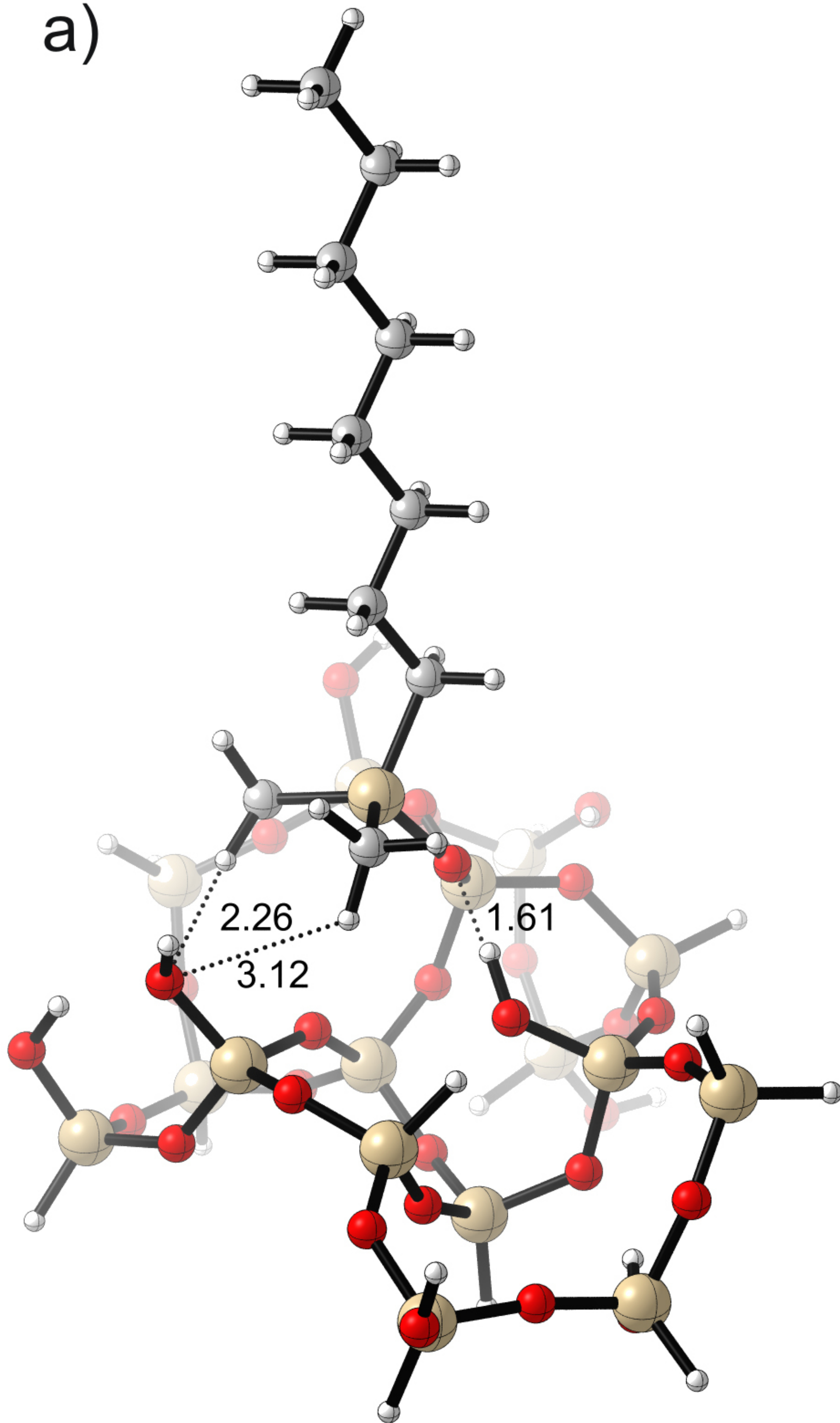
A



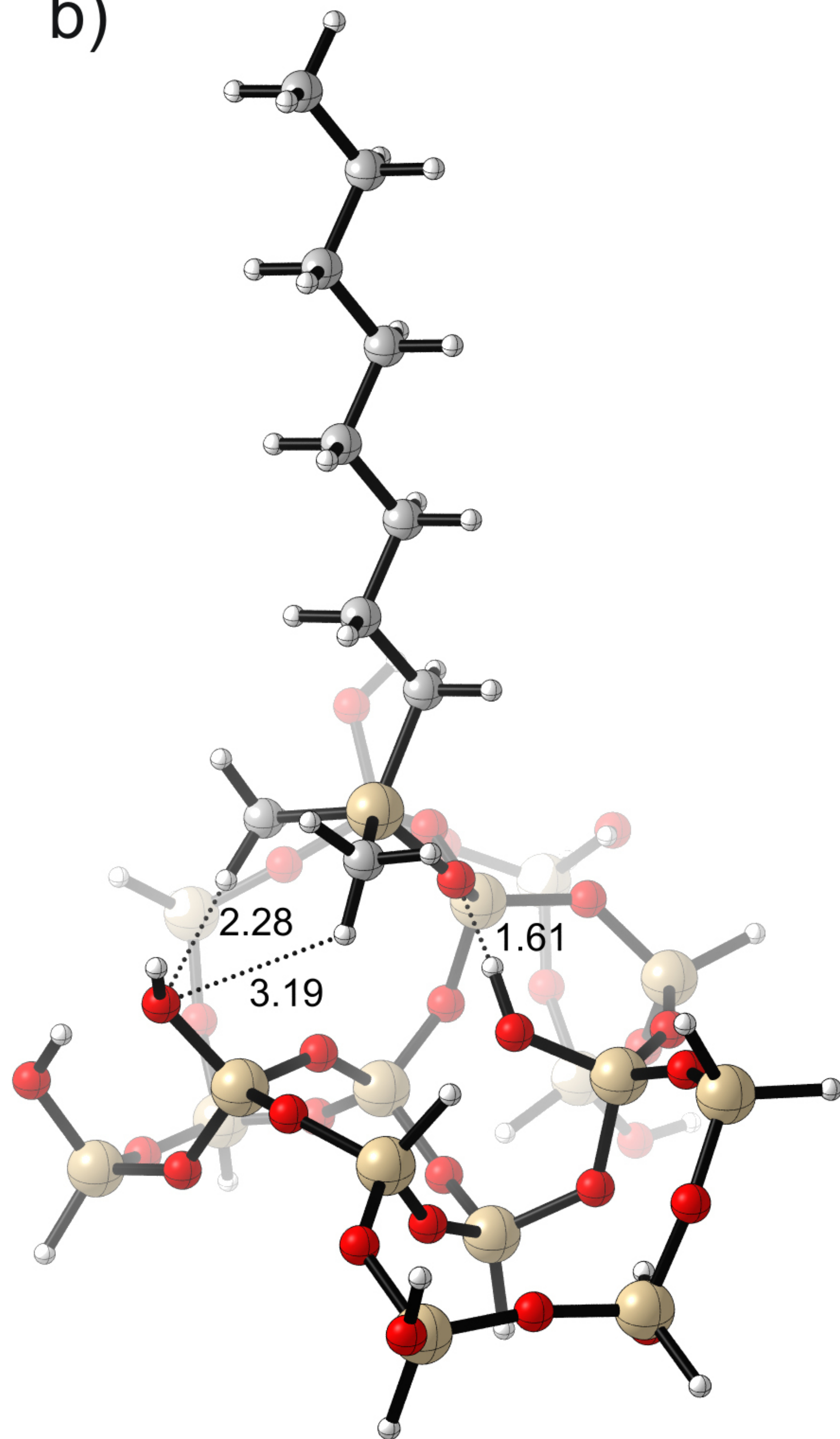
B



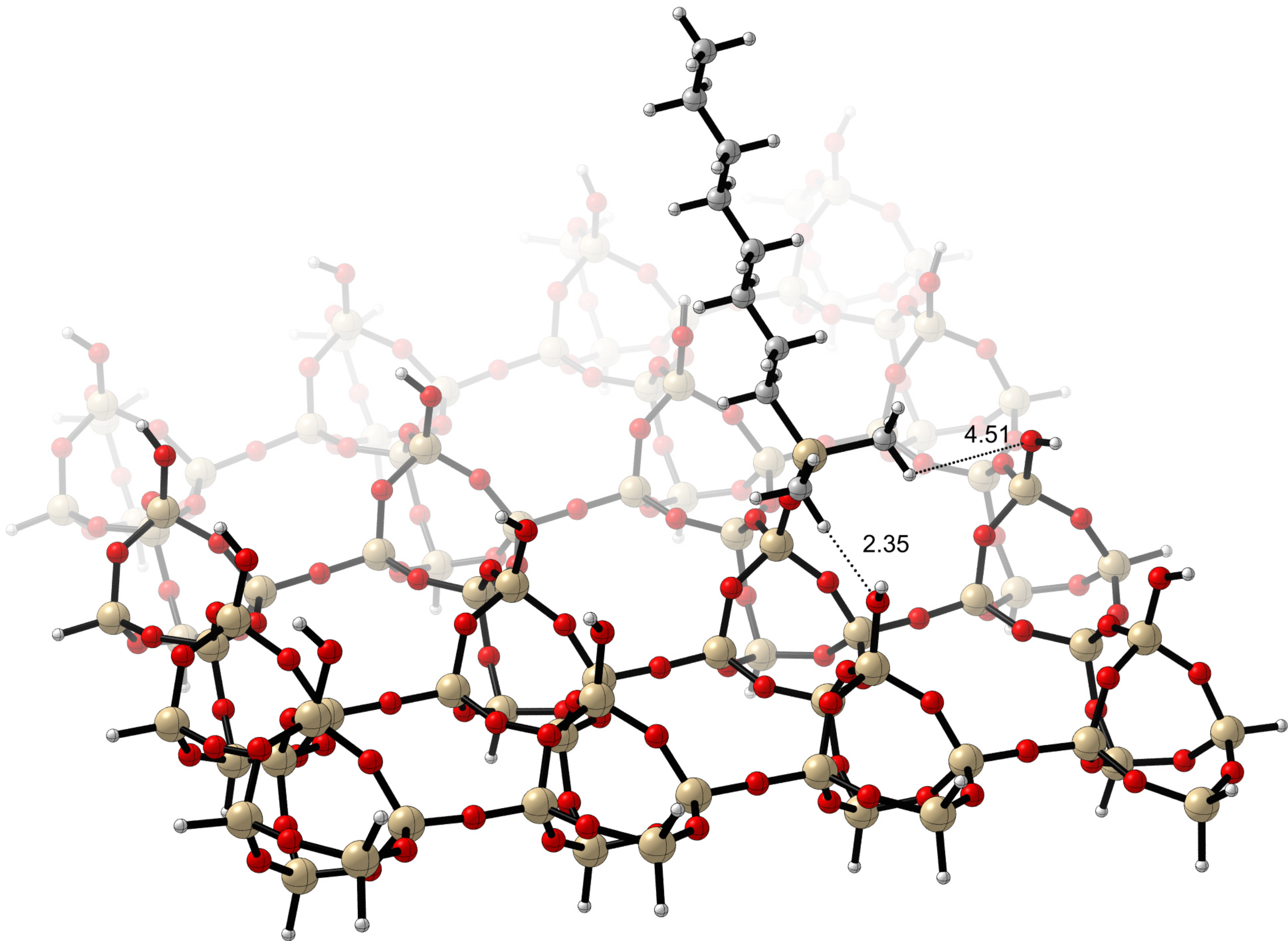
a)



b)



1
2
3
4
5
6
7
8
9
10
11
12
13
14
15
16
17
18
19
20
21
22
23
24
25
26
27
28
29
30
31
32
33
34
35
36
37
38
39
40
41
42
43
44
45
46
47
48
49
50
51
52
53
54
55
56
57
58
59
60



1
2
3
4
5
6
7
8
9
10
11
12
13
14
15
16
17
18
19
20
21
22
23
24
25
26
27
28
29
30
31
32
33
34
35
36
37
38
39
40
41
42
43
44
45
46
47
48
49
50
51
52
53
54
55
56
57
58
59
60